

Investigation of the Puzzling Abundance Pattern in the Stars of the Fornax Dwarf Spheroidal Galaxy

Hongjie Li^{1,2}, Wenyuan Cui¹ and Bo Zhang^{1,3}

1. *Department of Physics, Hebei Normal University, No. 20 East of South 2nd Ring Road, Shijiazhuang 050024, China*

2. *School of Sciences, Hebei University of Science and Technology, Shijiazhuang 050018, China*

ABSTRACT

Many works have found unusual characteristics of elemental abundances in nearby dwarf galaxies. This implies that there is a key factor of galactic evolution that is different from that of the Milky Way (MW). The chemical abundances of the stars in the Fornax dwarf spheroidal galaxy (Fornax dSph) provide excellent information for setting constraints on the models of the galactic chemical evolution. In this work, adopting the five-component approach, we fit the abundances of the Fornax dSph stars, including α elements, iron group elements and neutron-capture elements. For most sample stars, the relative contributions from the various processes to the elemental abundances are not usually in the MW proportions. We find that the contributions from massive stars to the primary α elements and iron group elements increase monotonously with increasing $[\text{Fe}/\text{H}]$. This means that the effect of the galactic wind is not strong enough to halt star formation and the contributions from massive stars to α elements did not halted for $[\text{Fe}/\text{H}] \lesssim -0.5$. The average contributed ratios of various processes between the dSph stars and the MW stars monotonously decrease with increasing progenitor mass. This is important evidence of a bottom-heavy initial mass function (IMF) for the Fornax dSph, compared to the MW. Considering a bottom-heavy IMF for the dSph, the observed relations of $[\alpha/\text{Fe}]$ versus $[\text{Fe}/\text{H}]$, $[\text{iron group}/\text{Fe}]$ versus $[\text{Fe}/\text{H}]$ and $[\text{neutron-capture}/\text{Fe}]$ versus $[\text{Fe}/\text{H}]$ for the dSph stars can be explained.

Subject headings: galaxies: abundances–galaxies: dwarf–stars: abundances

³Corresponding author. E-mail address: zhangbo@mail.hebtu.edu.cn

1. Introduction

Nearby galaxies can provide many important clues for us to understand the star formation history, evolution process and relation between them and the Milky Way (MW). In the past decade, the accurate abundance of dwarf spheroidal galaxies (dSphs) has allowed a detailed study of their star formation and chemical evolution histories (Tolstoy et al. 2003; Lanfranchi & Matteucci 2003, 2007; Lanfranchi et al. 2008). Some important chemical signatures, such as the lower $[\alpha/\text{Fe}]$ ratios, have been studied. D’Ercole & Brighenti (1999) found that the galactic winds can remove a large fraction of gas and the elements produced by massive stars, which would reduce the enrichment of the interstellar medium (ISM). Tolstoy et al. (2003) and Shetrone et al. (2003) suggested that the low abundance ratios could be due to a low star formation rate. Based on the study of chemical evolution of dSphs, Lanfranchi & Matteucci (2003) found that the low $[\alpha/\text{Fe}]$ could be explained quantitatively by a sudden decrease of star formation. Because of relatively shallow potential wells for dwarf galaxies, the strong galactic winds can remove a large fraction of the gas and, consequently, the star formation rate drops to a very low value. In this case, the enrichment of α elements by massive stars is almost halted and SNe Ia are left to contribute their production, such as iron group elements, due to longer lifetime. As a result, when the galactic winds occur, the $[\alpha/\text{Fe}]$ ratios decrease (Lanfranchi et al. 2006; Lanfranchi & Matteucci 2007; Lanfranchi et al. 2008).

Using the high resolution spectroscopy, Letarte et al. (2010) analyzed the elemental abundances of the red giant branch stars in the central region of the Fornax dwarf spheroidal galaxy (Fornax dSph). This analysis shows the lower ratios of $[\alpha/\text{Fe}]$, $[\text{Ni}/\text{Fe}]$ and $[\text{Cr}/\text{Fe}]$ compared with those in the MW stars. In contrast, the abundance of some neutron-capture elements, such as Ba and La, are enhanced. They found that their sample stars have unusually abundance patterns and that the Fornax dSph is a chemically complex system. The Fornax dSph is one of the dwarf spheroidal companions to the Milky Way. It is a luminous dwarf galaxy with a luminosity of $M_v = -13.0 \pm 0.3$ (Irwin & Hatzidimitriou 1995) and the second most massive dwarf galaxy satellites of our Galaxy with a total (dynamical) mass in the range $10^8 - 10^9 M_\odot$ (Mateo et al. 1991; Walker et al. 2006). Moreover, it shows a wider range of metallicity and multiple populations (e.g., Battaglia et al. (2006); Letarte et al. (2010)). The observed abundances of individual stars could provide an excellent opportunity to study the star formation history and complicated chemical evolution history of the Fornax dSph. Recently, Tsujimoto (2011) studied abundance trends in Fornax dSph and concluded that a different form of the initial mass function (IMF) is needed. He found that the lack of very massive stars ($M \gtrsim 25 M_\odot$) may explain the low $[\alpha/\text{Fe}]$ observed in the Fornax dSph. On the other hand, based on the analysis of the colour-magnitude diagrams and the spectroscopic metallicity distributions of individual red giant branch stars, de Boer et al.

(2012) studied the star formation history of the Fornax dSph. They found that although the Fornax dSph is dominated by intermediate age (1-10 Gyr) stellar populations, the star formation is clearly present at all ages, from 14 Gyr to 0.25 Gyr. This implies that the galactic wind effect is not intense enough to halt the star formation in the Fornax dSph.

Elements heavier than iron are mainly synthesized by neutron-capture process in two ways: one is the slow neutron-capture process (the s-process) and the other is the rapid neutron-capture process (the r-process) (Burbidge et al. 1957). The s-process is divided into the weak s-component and the main s-component. The weak s-process occurs in the massive stars ($M \gtrsim 10M_{\odot}$) undergoing core He burning and shell C burning (Käppeler et al. 1989; Raiteri et al. 1991, 1992, 1993; The et al. 2000). Otherwise, the main s-process elements are produced in the low- to intermediate-mass stars ($\approx 1.5-8M_{\odot}$) during the asymptotic giant branch (AGB) phase (Busso et al. 1999). Type II supernovae (SNe II) are usually considered to be the candidates in which the r-process nucleosynthesis occurs (Cowan et al. 1991; Sneden et al. 2008). Because of the large Eu overabundance ($[\text{Eu}/\text{Fe}] \sim 1.6$), two metal-poor stars CS 22892-052 and CS 31082-001 arose extensive attention. These two stars are called as “main r-process stars”, because their abundance patterns of the heavier neutron-capture elements match the solar-system r-process pattern well (e.g., Cowan et al. (1999); Truran et al. (2002); Wanajo & Ishimaru (2006); Sneden et al. (2008)). However, their lighter neutron-capture elements are too deficient to fit the solar-system’s r-process pattern. This implies that another process, which is referred to the “lighter element primary process” (Travaglio et al. 2004; Cowan et al. 2005; Cowan & Sneden 2006) or “weak r-process” (Ishimaru et al. 2005), is needed. The abundance patterns of weak r-process stars, HD 122563 and HD 88609, show an excess of lighter neutron-capture elements and a deficiency of heavier neutron-capture elements (Westin et al. 2000; Johnson 2002; Honda et al. 2004).

Observational abundances of metal-poor stars in the MW show that the heavier neutron-capture elements and light elements are not produced in the same sites (Johnson 2002; Sneden et al. 2003; Honda et al. 2004). This implies that the main r-process should occur in O-Ne-Mg core-collapse SNe II with progenitors of $8-10M_{\odot}$ (Qian & Wasserburg 2007). Otherwise, the weak r-process elements are coupled with the light elements and iron group elements (Qian & Wasserburg 2002, 2007; Izutani et al. 2009). The primary light elements and iron group elements (i.e., the yields independent of initial metallicity approximately) are produced in massive stars with $M \gtrsim 10M_{\odot}$ (Heger & Woosley 2010). Montes et al. (2007) analyzed the abundance of metal-poor stars and found that the weak r-process abundance pattern is uniform and unique. Based on the observed abundances of weak r-process stars and the main r-process stars, Li et al. (2013) derived the abundances of weak r-process and main r-process using an iterative method and extended “the weak r-process component” to

primary light elements and primary iron group elements. They found that the abundances in all metal-poor stars contain the contributions from the two r-processes.

Because stars of different mass contribute different elements to the dSph on different timescales, the abundances of individual stars contain the contributions from various astrophysical processes and are the integrated results over the lifetime of the system since the stars were born. In order to reveal the complicated star formation history and evolution process of Fornax dSph, it is important to analyze the elemental abundances in detail, including α elements, iron group elements and neutron-capture elements. These reasons inspired us to study the abundance of the dSph stars. In this case, the quantitative decomposing stellar elemental abundances of the contributions from various astrophysical processes are significant. In this paper, we study the astrophysical origins that reproduce the abundance pattern of 56 stars in the Fornax dSph, in which the α elements, iron group elements, lighter neutron-capture elements and heavier neutron-capture elements have been observed, and we analyze the relative contributions from the individual processes. The five-component abundance approach is described in Section 2. In Section 3, the analysis of calculated results are presented. Section 4 is our conclusions.

2. Abundance analysis approach of the stars in the dSph and MW

Several previous studies on the abundances of neutron-capture elements have indicated that for most stars, the observed abundances of the heavy elements cannot be matched by only one neutron-capture process (Travaglio et al. 1999, 2004; Allen & Barbuy 2006). One of our major goals is to explore the astrophysical origin of elements, including light elements, iron group elements and neutron-capture elements, in the stars of the Fornax dSph by comparing the observed abundances with the predicted contributions of various astrophysical processes. The i th element abundance can be calculated as

$$N_i([Fe/H]) = (C_{r,m}N_{i,r,m} + C_{pri}N_{i,pri} + C_{s,m}N_{i,s,m} + C_{sec}N_{i,sec} + C_{Ia}N_{i,Ia}) \times 10^{[Fe/H]} \quad (1)$$

where $N_{i,r,m}$, $N_{i,pri}$, $N_{i,s,m}$, $N_{i,sec}$ and $N_{i,Ia}$ are the abundances of the i th element produced by the main r-process, the primary process in massive stars, the main s-process, the secondary process in massive stars, and SNe Ia, respectively, which have been normalized to abundances of the solar system; The component coefficients $C_{r,m}$, C_{pri} , $C_{s,m}$, C_{sec} and C_{Ia} represent the relative contributions from the main r-process, the primary process, the main s-process, the secondary process and SNe Ia, respectively. Using the five component coefficients, we can determine the relative contributions of each process to the elemental abun-

dances and then compare them with the corresponding component coefficients of the solar system (or $[\text{Fe}/\text{H}]=0$) in which $C_{r,m}=C_{pri}=C_{s,m}=C_{sec}=C_{Ia}=1$. However, these component coefficients are not usually expected to be equal to each other. For example, the abundances of neutron-capture elements in the interstellar gas that formed very metal-deficient stars is expected to come from mostly r-process events (Montes et al. 2007). This method was used by Shen et al. (2013) to study the abundances of Ba stars. The abundances of $N_{i,Ia}$ are taken from Timmes et al. (1995), in which the abundances of Fe, Cu and Zn are adopted from Mishenina et al. (2002).

Observational abundances of metal-poor stars in the MW show that the weak r-process elements are coupled with the primary light elements and iron group elements (Qian & Wasserburg 2002, 2007; Izutani et al. 2009). Massive stars ($M \gtrsim 10M_{\odot}$) are the astrophysical origins of the primary elements, including the primary light elements, iron group elements and weak r-process elements, and provide significant contributions to the solar abundances for these elements. Note that the mass range of progenitors in which the light elements and iron group elements were produced should be different from the progenitor mass range of SNe II in which the weak r-process elements were produced. The sites of weak r-process should be the Fe-core-collapse SNe II with progenitors of mainly about $11\text{-}25M_{\odot}$ (Qian & Wasserburg 2007) from which the primary light elements and iron group elements are also ejected. However, more massive stars ($M \gtrsim 25M_{\odot}$) can also produce the primary light elements and iron group elements (Heger & Woosley 2010). In this case, the contributions from the more massive stars should have existed in the observational abundances of the metal-poor stars and are difficult to separated out. Because the contributions from the more massive stars, which have shorter lifetime, are always present at various times, the light elements and iron group elements in “the weak r-process component” derived from the weak r-process stars, HD 122563 and HD 88609, should contain the contributions from the more massive stars. In this work, the weak r-process component derived by Li et al. (2013) is called the “primary component”, since the associated light elements, iron group elements and the weak r-process elements are produced in massive stars as primary yields. Note that the best-fitted results of the metal-poor stars with metallicity range $-3.0 < [\text{Fe}/\text{H}] < -2.0$ for the light elements and iron group elements by Li et al. (2013) imply that a more complete analysis using the abundances of more metal-poor stars would likely offer only minor corrections to the abundances pattern of the primary component. The abundances of main r-process $N_{i,r,m}$ are adopted from Li et al. (2013).

Due to the secondary-like nature of major neutron source $^{22}\text{Ne}(\alpha, n)^{25}\text{Mg}$, the contributions from weak s-process are negligible for metal-poor stars (Travaglio et al. 2004). The abundances of weak s-process are taken from Travaglio et al. (2004) at $[\text{Fe}/\text{H}]=0$. The ratios of $[\alpha/\text{Fe}]$ observed for the MW stars show a plateau at $[\text{Fe}/\text{H}] \lesssim -1$, which means that the α

elements are produced mainly by the primary-like mechanisms. Based on nucleosynthesis calculations, Woosley et al. (2002) found that the effect of metallicity on the production of α elements in massive stars is mild. However, the observed increase in some odd-Z elements and iron group elements toward high [Fe/H] is the effect of metallicity on nucleosynthesis (Mishenina et al. 2002; Kobayashi et al. 2006; Feltzing et al. 2007). Nucleosynthesis calculations for massive stars show that the yields of some odd-Z elements (e.g., Na and Al) and iron group elements (e.g., Mn) increased with increasing metallicity (Woosley & Weaver 1995; Kobayashi et al. 2006). The astrophysical sites of, and dominant contributing processes to, some iron group elements still have not been reliably established. Mishenina et al. (2002) found that the abundance of iron group element Cu in the MW contains the contributions from the primary process and secondary process (i.e., the yields which increase with increasing initial metallicity) in massive stars. According to estimate of Mishenina et al. (2002), the contributed fraction from the secondary process in massive stars for Cu is reached about 25% for the solar system. Allen & Porto (2011) have found that for disk stars, although the iron group elements are mostly synthesized by SNe Ia, the secondary-like contributions from the massive stars are non-negligible. Shen et al. (2013) found that, for light elements and iron group elements, the abundances in the solar system are higher than the sum of contributions from primary component and SNe Ia, because the contributions from secondary-like yields produced in the massive stars are not included. In this work, we obtain the secondary-like abundances for the light elements and iron group elements by subtracting the sum of the contributions of primary-like yields (adopted from Li et al. (2013)), SNe Ia (adopted from Timmes et al. (1995)) and main s-process component (adopted from Travaglio et al. (2004)) from the solar system abundances (adopted from Anders & Grevesse (1989)). This procedure ensures that the sum of the abundances of four components is not overproduced with respect to solar. Because the weak s-process elements are also produced in massive stars and have a secondary nature, the secondary-like abundances of light elements and iron group elements should be tightly related to the weak s-process abundances.

The secondary light elements, iron group elements and the weak s-process elements are produced in the massive stars ($M \gtrsim 10M_{\odot}$) (Käppeler et al. 1989; Raiteri et al. 1993; The et al. 2000; Mishenina et al. 2002; Kobayashi et al. 2006; Pignatari et al. 2010). However, the mass range of the stars in which the light elements and iron group elements were produced should be different from those of the stars in which the weak s-process elements were produced. The sites of the weak s-process (and the part of secondary-like yields for the light elements and iron group elements) are mainly the massive stars with $\sim 10 - 30M_{\odot}$ (The et al. 2007). However, the more massive stars ($M > 30M_{\odot}$) can also produce the secondary light elements and iron group elements. The contributions from the more massive stars are difficult to distinguish in the observed abundances of the sample stars, because

the timescale is long enough to permit all massive stars to eject their productions for higher metallicities ($[\text{Fe}/\text{H}] \gtrsim -2.0$). Recently, Ono et al. (2012) reported that the weak s-process also occurs in star with $70M_{\odot}$. This would mean that the mass range of stars in which the weak s-process occurs may be similar to those of stars in which the secondary light elements and iron group elements were produced. Based on the discussions above, we combined the secondary-like abundances for the light elements and iron-group elements with weak s-process abundances as “the secondary component”. The secondary component $N_{i,sec}$ contains the abundances of the light elements, iron group elements and the weak s-process elements.

Based on the observations, Letarte et al. (2010) found that compare to the MW, the ratios of $[\text{Ba}/\text{Fe}]$ and $[\text{Y}/\text{Fe}]$ in the dSph show larger dispersions and $[\text{Ba}/\text{Y}]$ are exceedingly high. This means that the ISM in the dSph is chemical inhomogeneous and the abundance pattern of s-process elements of a newly-formed star was polluted by the winds of low-mass AGB stars with low-metallicity in the vicinity. In this case, the s-process nucleosynthesis favors heavier nuclei over lighter ones, since more neutrons can be captured by an iron seed nucleus (Busso et al. 2001). Obviously, there are some differences in the chemical evolution characteristics between the dSph and the MW, which lead to the different s-process abundance patterns between the dSph and the Milky Way. So, the s-process abundance patterns of the MW are not adequate to used in the dSph stars. Considering the wide range of metallicity of the sample stars ($-1.4 \lesssim [\text{Fe}/\text{H}] \lesssim -0.5$) in dSph, the abundance pattern of $N_{i,s,m}$ in equation (1) is calculated as the mixing of the main s-process abundance produced by low-mass AGB stars with $[\text{Fe}/\text{H}]=-1.0$ and $[\text{Fe}/\text{H}]=-0.6$, which are given by Busso et al. (2001). We calculate the main s-process abundance using the equation:

$$C_{s,m}N_{i,s,m} = C_1N_{i,s,m}([\text{Fe}/\text{H}] = -1) + C_2N_{i,s,m}([\text{Fe}/\text{H}] = -0.6) \quad (2)$$

in which $N_{i,s,m}$, $N_{i,s,m}([\text{Fe}/\text{H}]=-1)$ and $N_{i,s,m}([\text{Fe}/\text{H}]=-0.6)$ have been normalized to the main s-process component of Ba in solar system (Arlandini et al. 1999). In this case, $C_{s,m}=C_1+C_2$. By comparison, for the stars in the MW, the adopted metallicity-dependent abundance pattern $N_{i,s,m}$ in equation (1) is taken from the main s-process abundance given by Travaglio et al. (1999) (see their Fig. 6-Fig. 12) and Serminato et al. (2009) (see their Fig. 3-Fig. 6), which included the contributions of low- to intermediate-mass AGB stars ($\sim 1.5 - 8M_{\odot}$) and also has been normalized to the main s-process abundance of Ba in solar system.

In equation (1), we have defined five component coefficients. We can obtain them by looking for the minimum χ^2 . The reduced χ^2 is defined as

$$\chi^2 = \sum_{i=1}^K \frac{(\log N_{i,obs} - \log N_{i,cal})^2}{(\Delta \log N_{i,obs})^2 (K - K_{free})} \quad (3)$$

where $N_{i,cal}$ is the abundance calculated from equation (1), $\log N_{i,obs}$ and $\Delta \log N_{i,obs}$ are the observed abundance and error of the i th element, respectively, K is the number of elements applied in the fit and K_{free} is the number of free parameters. Here, $K_{free}=5$, because equation (1) contains five component coefficients. Using component coefficients, we can determine the relative contributions of each individual process to the stellar abundances. Moreover, we can compare the derived component coefficients with the corresponding coefficients of the solar system in which all of them are equal to 1. For the sample stars, the five component coefficients are not equal to each other, because their elemental abundances are not in solar proportions.

3. Results and Discussion

In this work we analyze the observational constraints provided by the elemental abundances of the stars in the Fornax dSph to investigate the relative contributions from the individual process. Using the observed data of Fornax dSph stars (Letarte et al. 2010), the fitted parameters can be obtained. The derived component coefficients and χ^2 are listed in Table 1. A comparison between the abundance-decomposed results of Fornax dSph stars and the MW stars with a similar metallicity range is necessary to ascertain whether the elements in the two galaxies have a similar origin or a different chemical evolution history. Using the observed data of the MW stars (Mishenina & Kovtyukh 2001; Reddy et al. 2003, 2006), the derived component coefficients and χ^2 are listed in Table 2. The [Fe/H] distributions of the dSph stars and the MW sample stars are compared in Figure 1. One can see that the dSph stars have a similar distribution of [Fe/H] to that of the Milky Way.

As two examples, the calculated best-fitting results for the dSph star BL185 and the MW star HIP 72803 are shown in Fig. 2. The solid lines and filled circles represent the calculated results and the observed abundances, respectively. The top panels of Figs. 3(a) and 3(b) show the individual relative offsets ($\Delta \log \varepsilon = \log \varepsilon_{cal} - \log \varepsilon_{obs}$) for the dSph stars and MW stars, respectively. The bottom panels of Figs. 3(a) and 3(b) show the root-mean-square offset in $\log \varepsilon$. Typical observational uncertainties in $\log \varepsilon$ are $\sim 0.2 - 0.3$ dex (dash lines). It could be found from Fig. 3 that the individual relative offsets are mostly smaller than 0.30 dex and the root-mean-square offset is consistent with zero. The calculated results shown in Figs. 2 and 3 confirm the validity of the abundance approach adopted in this work.

In the study of the abundances of the dSph stars, the component coefficient as the function of metallicity is very important, since it shows the chemical evolution features of the dSph. If $C_k > 1$ (or $C_k < 1$, $k=r,m$; pri; s,m; sec and Ia), the contribution from the process corresponding to the elemental abundances is larger (or less) than that in the solar

system, after excluding the effect of metallicity. These component coefficients are not usually expected to be equal to each other, because the relative contributions of these components are not always in proportion to those of the solar-system. The left panel and right panel in Fig. 4 show the component coefficients $C_{r,m}$, C_{pri} , $C_{s,m}$, C_{sec} and C_{Ia} as a function of $[\text{Fe}/\text{H}]$ for the dSph stars and the MW stars, respectively. In this work, the adopted primary component and secondary component contain the abundances of light elements, iron group elements and neutron-capture elements. For neutron-capture elements, C_{pri} and C_{sec} represent the component coefficients of weak r- and weak s-process, respectively. For light elements and iron group elements, C_{pri} and C_{sec} represent the contributions from primary-like and secondary-like yields in massive stars, respectively.

For detailed comparisons, Figs. 5 (a)-5 (e) show the distributions of five component coefficients obtained for the dSph stars (solid lines) and the MW stars (dash lines). There is a tendency for the component coefficients $C_{r,m}$, $C_{s,m}$ and C_{Ia} of the dSph stars to be larger than those of the MW sample stars. This means that the contributions from main r-process, main s-process and SNe Ia to the abundances of the dSph stars are larger than those of the MW stars. However, a trend exists wherein the component coefficients C_{pri} and C_{sec} of the dSph stars are smaller than those of the MW stars. This means that the contributions from the primary process (or weak r-process) and the secondary process (or weak s-process) to the dSph stars are smaller than those to the MW stars.

The stellar initial mass function (IMF) is an important function of a galaxy, which can be applied extensively to various aspects of astrophysics. The IMF of a dwarf galaxy may depend on its dynamics and kinematics characteristics (Dutton et al. 2012) and directly effect the chemical abundances of the dwarf galaxy stars. Because the α elements, iron group elements, lighter neutron-capture elements and heavier neutron-capture elements have different astrophysical origins, one could investigate the IMF using the contributions of various processes to the abundances of the dSph stars. Recall that the main r-process should occur in O-Ne-Mg core-collapse SNe II with progenitors of $8\text{-}10M_{\odot}$ and the primary elements (including primary light elements, iron group elements and weak r-elements) are produced in the massive stars with $M \gtrsim 10M_{\odot}$. On the other hand, the secondary elements (including secondary light elements, iron group elements and weak s-elements) are produced in the massive stars ($M \gtrsim 10M_{\odot}$) and the main s-process elements are mainly produced in the low-mass AGB stars ($\sim 1.5\text{-}3M_{\odot}$). In Fig. 6, we show the ratios of the average component coefficient between the dSph stars and the MW stars as function of progenitor mass. The ratios monotonously decrease with the increasing progenitor mass. This means that, compare to the MW, the bottom-heavy IMF for the Fonax dSph is strongly suggested.

Because stars of various mass contribute different elements to the dSph on different

timescales, the observed abundances of the sample stars are the integrated results over the lifetime of the system since the stars were born. In order to make a progress in understanding the chemical evolution of Fornax dSph in greater detail, we derive the component ratios of the individual process (i.e., $[\text{element}/\text{H}]_k$ ($k=r,m; \text{pri}; s,m; \text{sec}; \text{SNe Ia}$)) with various metallicities and compare them with those of the MW stars. In Figs. 7-11, we show the component ratios of Fe, α element Mg, iron group element Ni, lighter neutron-capture element Y and heavier neutron-capture element Ba. For ease of comparison with the solar system, we add some lines in these figures. The dash dotted lines, solid lines, short dotted lines, dash lines, and dotted lines represent the solar component ratios of the main r-process, primary process, main s-process, secondary process and SNe Ia, respectively. From Fig. 7 (b), we can see that for the MW stars, the contributions from the primary-like yields to $[\text{Fe}/\text{H}]$ ratios are larger than those from SNe Ia and the secondary-like yields. However, Fig. 7 (a) shows that the Fe abundances for the dSph stars predominantly come from SNe Ia and the ratios of SNe Ia have reached the solar ratio. These results are consistent with the bottom-heavy IMF for the dSph. In this case, the contributions from the primary-like yields and secondary-like yields produced in the massive stars to the dSph are smaller than corresponding contributions to the Milky Way.

From Fig. 8 (b) we can see that, for the MW stars, the Mg abundances predominantly come from the primary process and the ratios are larger than the solar ratio. In Fig. 8 (a), we find that the Mg abundances in the dSph stars also mainly come from the primary process in the massive stars. However, the ratios of the primary process of the dSph stars are close to that of the solar system and lower than those of the MW stars. From Fig. 8 (a) we can see that the ratios of $[\text{Mg}/\text{H}]_{\text{pri}}$, which represent the contributions from massive stars to the primary yields, increase monotonously with increasing $[\text{Fe}/\text{H}]$. This means that the massive stars have continued chemical enrichment during the dSph evolution, even though they do not dominate the Fe enrichment. In other words, for the Fornax dSph, the stars formed at all ages and the contributions from the massive stars to α elements did not stop, at least for $[\text{Fe}/\text{H}]$ reaching to -0.5. The continual contributions from the massive stars to the primary yields of iron group elements for the metallicity range from $[\text{Fe}/\text{H}]=-1.0$ to $[\text{Fe}/\text{H}]=-0.5$ can also be found from Figure 7 and Figure 9 for iron group elements Fe and Ni. The correlation between $[\text{Mg}/\text{H}]_{\text{pri}}$ and $[\text{Fe}/\text{H}]$ obtained from this work is a significant evidence that the effect of the galactic wind is not strong enough to halt the star formation in the Fornax dSph. Because of the bottom-heavy IMF for the dSph, the contributions from the primary-like yields produced in the massive stars to the dSph are smaller than corresponding contributions to the Milky Way. Letarte et al. (2010) have found that the observed $[\text{Mg}/\text{Fe}]$ of the dSph stars are lower than those of the MW stars and close to the solar ratio (see their Fig. 10). After considering the bottom-heavy IMF for the dSph, the abundance ratios of α

elements (e.g., Mg, Si, Ca and Ti) observed in the dSph stars can be explained.

In Fig. 9 (b), for the MW stars, the calculated results imply that the Ni abundances mainly come from the contributions of the primary process and secondary process. The component ratios of the primary process are larger than that of the solar primary ratio, and the component ratios of the secondary process have reached the solar secondary ratio at $[\text{Fe}/\text{H}] \sim -0.8$. Although the component ratios of SNe Ia are smaller than the solar ratio, the component ratios of the primary- and the secondary-like yields produced in massive stars are larger than the corresponding solar ratios. These are the reasons for the observed $[\text{Ni}/\text{Fe}] \approx 0$ (see Fig. 12 in Letarte et al. (2010)) in the MW stars. In contrast to the Milky Way, from Fig. 9 (a) we can see that for the dSph stars, the component ratios of SNe Ia for Ni are larger than those of the primary process and the secondary process. The ratios of the SNe Ia are close to the solar ratio of the SNe Ia, and the ratios of the secondary process are lower than the solar secondary ratio by about 0.5 dex. Letarte et al. (2010) have found that the observed $[\text{Ni}/\text{Fe}]$ of the dSph stars are lower than those of the MW stars and the solar system (see their Fig. 12). These results are consistent with a bottom-heavy IMF for the dSph. In this case, although the component ratios of SNe Ia have reached the solar ratio, the component ratios of the primary process and the secondary process for the dSph are smaller than the corresponding ratios of the Milky Way. These are the reasons of observed $[\text{Ni}/\text{Fe}] < 0$ for the Fornax dSph stars. The abundance ratios of another iron group element Cr observed in the dSph stars can also be explained after considering the bottom-heavy IMF.

From Fig. 10(b), we can see that for the MW stars, the Y abundances mainly come from the weak r-process and main s-process. The component ratios of the weak r-process are larger than the solar ratio of weak r-process and the component ratios of the main s-process are smaller than the solar ratio of main s-process. On the other hand, from Fig. 10 (a) we can see that, for most dSph stars, contributions from the main s-process exceed main r-process and weak r-process contributions, and the weak s-process contributions are negligible at all metallicities. The ratios of the main s-process have reached the solar ratio at $[\text{Fe}/\text{H}] \gtrsim -0.9$. Because of the bottom-heavy IMF, the contributions from main s-process in the AGB stars to the dSph are larger than the corresponding contributions to the MW. Although the average value of $[\text{Y}/\text{Fe}]$ for dSph stars is close to that of the MW, the proportions contributed from main s-process, main r-process and weak r-process are obviously different.

From Fig. 11(b) we can see that for the MW stars, the Ba abundances mainly come from the main r-process and main s-process. The component ratios of the main r-process are larger than the solar ratio of main r-process and the ratios of the main s-process are slightly lower than the solar ratio of the main s-process. From Fig. 11(a) we can see that, for most dSph stars, contributions from the main s-process exceed contributions from main

r-process for $[\text{Fe}/\text{H}] > -1.0$ and begin to drive $[\text{Ba}/\text{H}]$ upward to $[\text{Ba}/\text{H}] = 0$. In this case, the ratios of the main s-process for Fornax stars are larger than those of the solar system and the MW stars. Letarte et al. (2010) have found that the observed $[\text{Ba}/\text{Fe}]$ of most dSph stars are higher than those of the MW stars and the solar system (see their Fig. 14). It is natural result that the contributions of main s-process produced in AGB stars to the dSph are larger than corresponding contributions to the Milky Way due to the bottom-heavy IMF of the dSph. Similar to Ba, the La abundance ratios of the dSph stars can be explained. Letarte et al. (2010) have found that $[\text{Eu}/\text{Fe}]$ of dSph stars are at the same levels observed in the MW stars for the same $[\text{Fe}/\text{H}]$. Our calculated results about main r-process component coefficients are consistent with their findings.

The apparent rise of $[\text{La}/\text{Fe}]$ or $[\text{Ba}/\text{Fe}]$ observed in Fornax dSph or Sagittarius dSph is due to pollution by AGB stellar wind. The calculated results presented by Lanfranchi et al. (2008) show that $[\text{La}/\text{Fe}]$ (or $[\text{Ba}/\text{Fe}]$) decrease slightly at high metallicities, which is due to the effects of galactic winds on the star formation rate. This means that there is a discrepancy between predictions of the chemical evolution model and observations. Furthermore, Lanfranchi et al. (2008) have found that an increase in the yields of La in AGB stars by a factor that is smaller than four is not enough to match the observed ratios. However, they reported that if the s-process yields of the AGB stars were increased considerably, the yields could not be used in the MW and the solar system correctly. Obviously, there is other reason to explain the rise of $[\text{Ba}/\text{Fe}]$ or $[\text{La}/\text{Fe}]$ observed in the dSphs.

Historically, variations in the IMF have been proposed to reduce the chemical enrichment from massive stars (Matteucci & Chiosi 1983). The truncated IMF has been used as a possible cause of lowering $[\alpha/\text{Fe}]$ in dwarfs (Tolstoy et al. 2003). Because the s-process yields should mainly be dependent on the initial mass and metallicity of the low mass AGB stars, the average yields of the AGB stars with the same initial mass and metallicity as the dSph should be similar to those of the MW. In this case, the rise of $[\text{Ba}/\text{Fe}]$ or $[\text{La}/\text{Fe}]$ observed in the dSphs should be attributed to contributions from the larger number of AGB stars. So, the abundances of s-process elements, Ba and La, in the dSph can be used to constrain the number of AGB stars that have polluted the gas in which the star formed and, thus constrain the IMF. It is interesting to note that, based on our calculation, the ratio of the average main s-process coefficient between the Fornax dSph and the MW is about 5.5, which is close to the increased factor of the AGB yields reported by Lanfranchi et al. (2008). Our calculated results mean that the reason for the rise of $[\text{Ba}/\text{Fe}]$ or $[\text{La}/\text{Fe}]$ observed in the dSphs is the bottom-heavy IMF, which favors a larger number of low-mass AGB stars.

4. Conclusions

In dSphs, nearly all chemical evolution and nucleosynthetic information is in the elemental abundances of stars with various metallicities. In this work, we investigate the astrophysical origins of the observed abundances of Fornax dSph stars and derive the relative contributions from the individual astrophysical process. Our results can be summarized as follows:

1. Adopting the five-component approach, the abundances of most sample stars, including α elements, iron group elements, lighter and heavier neutron-capture elements, can be fitted. The component coefficients of the main r-process, main s-process and secondary process of most dSph stars are different from those of the solar system. However, the component coefficients of primary process and SNe Ia are close to those of the solar system.

2. The component coefficients of the main s-process, secondary process, primary process and SNe Ia of the dSph stars are obviously different from those of MW stars with similar range of metallicity. The component coefficients of main r-process, main s-process and SNe Ia of most dSph stars are larger than those of the MW stars. This means that the contributions from main r-process, main s-process and SNe Ia to the dSph stars are larger than those to the MW stars. However, there are the trends for the dSph stars with smaller $C_{r,w}$, and $C_{s,w}$. This implies that for the dSph stars, the contributions from primary process and secondary process are smaller than the corresponding contribution for the MW stars.

3. The detailed abundance trends of five components for Fornax dSph could provide the information on the chemical enrichment history. We find that the contribution from massive stars as the primary yields of α elements and iron group elements increases monotonously with increasing $[\text{Fe}/\text{H}]$. This means that the star formed, including massive stars, at all ages and the contributions from the massive stars to α elements did not halted, at least until $[\text{Fe}/\text{H}]$ reached -0.5. These correlations provide the significant evidence that the effect of the galactic wind is not strong enough to halt the star formation in Fornax for $[\text{Fe}/\text{H}] \lesssim -0.5$.

4. The ratios of average component coefficient between the dSph stars and the MW stars monotonously decrease with the increasing progenitor mass. The correlation is significant evidence of the bottom-heavy IMF for the Fonax dSph, compared to the Milky Way.

5. Although Fornax dSph stars have a range of metallicity similar to the MW sample stars, the contribution proportions for Fe from various astrophysical processes of Fornax dSph stars are different with those of the MW stars. For the MW stars the contributions of the primary-like yields to Fe are larger than those of SNe Ia and the secondary-like yields. However, the Fe abundances in the dSph stars predominantly come from SNe Ia. This means that the contributions from the massive stars to the dSph are smaller than corresponding

contributions to the MW, which is consistent with the bottom-heavy IMF for the dSph.

6. Although Mg abundances predominantly come from the contributions of the primary process for both the MW stars and the Fornax dSph stars, the ratios of the primary process of the dSph stars are close to that of the solar system and lower than those of the MW stars. This suggests that the contributions of the primary-like yields produced in the massive stars to the dSph are smaller than the corresponding contributions to the MW. After considering the bottom-heavy IMF for the dSph, the lower $[\alpha/\text{Fe}]$ observed in the dSph stars can be explained.

7. For the MW stars, the abundances of the iron group element Ni mainly come from the primary process and secondary process. However, for the dSph stars, the component ratios of SNe Ia for Ni are larger than those of the primary process and the secondary process. Although the component ratios of SNe Ia has reached the solar system ratio, the component ratios of the primary process and the secondary process for the dSph are smaller than corresponding ratios of the MW. These are the reasons for observed $[\text{Ni}/\text{Fe}] < 0$ for Fornax dSph stars and are consistent with the bottom-heavy IMF.

8. For the MW stars, the abundances of lighter neutron-capture element Y mainly come from the weak r-process and main s-process. On the other hand, for most dSph stars, the contributions from the main s-process exceed the contributions from main r-process and weak r-process. The contributions from weak s-process can be negligible at all metallicities. Although the average value of $[\text{Y}/\text{Fe}]$ for dSph stars is close to that of the MW stars, the contributed proportions of the main s-process, main r-process and weak r-process are obviously different with those of the MW stars.

9. Because there are some differences in the s-process abundance characteristics between the dSph and the MW, the s-process abundance patterns of the MW are not adequate to used in the dSph stars. By adopting the mixing of the main s-process abundance produced by low-mass AGB stars with $[\text{Fe}/\text{H}] = -1.0$ and $[\text{Fe}/\text{H}] = -0.6$ presented by Busso et al. (2001), the abundances of the s-process elements, Ba and Y, can be fitted. The fitted results mean that the s-process elements in the dSph predominantly come from the low-mass AGB stars, which is consistent with the suggestion of the bottom-heavy IMF for the Fornax dSph.

10. For the MW stars, the abundances of the heavier neutron-capture element Ba mainly come from the contributions of the main r-process and main s-process. On the other hand, for the most dSph stars, contributions from the main s-process to Ba exceed contributions from the main r-process for $[\text{Fe}/\text{H}] > -1.0$ and begin to drive $[\text{Ba}/\text{H}]$ upward to $[\text{Ba}/\text{H}] = 0$. The rise of $[\text{Ba}/\text{Fe}]$ or $[\text{La}/\text{Fe}]$ observed in Fornax dSph can be attributed to contributions from the larger number of AGB stars. It is a natural result that the contributions of main

s-process produced in the low-mass AGB stars to the dSph are larger than corresponding contributions to the Milky Way due to the bottom-heavy IMF of the dSph.

Our abundance approach is based on the abundance patterns of the main r-process, main s-process, SNe Ia, primary process and secondary process to decompose stellar elemental abundances, rather than the traditional galactic chemical evolution model which integrates stellar yields beginning from early galaxies. This procedure allows us to use available elemental abundances to investigate their astrophysical origins and chemical evolution when each contribution is showed as a function of metallicity. We hope that the results here will provide a useful guide for more complete chemical evolution models of Fornax dSph. Obviously, a more precise knowledge about the elemental abundances in the dSph stars is needed.

This work has been supported by the National Natural Science Foundation of China under Grant No. 11273011, U1231119, 10973006 and 11003002, the Science Foundation of Hebei Normal University under Grant No. L2009Z04, the Natural Science Foundation of Hebei Province under Grant No. A2009000251, A2011205102, Science and Technology Supporting Project of Hebei Province under Grant No. 12211013D and the Program for Excellent Innovative Talents in University of Hebei Province under Grant No. CPRC034.

REFERENCES

- Allen, D. M., & Barbuy, B. 2006, *A&A*, 454, 917
- Allen, D. M., & Porto de Mello, G. F. 2011, *A&A*, 525, 63
- Anders, E., & Grevesse, N. 1989, *Geochim. Cosmochim. Acta*, 53, 197
- Arlandini, C., Käppeler, F., Wisshak, K., Gallino, R., Lugaro, M., Busso, M., & Straniero, O. 1999, *ApJ*, 525, 886
- Battaglia, G., et al. 2006, *A&A*, 459, 423
- Burbidge, E. M., Burbidge, G. R., Fowler, W. A., & Hoyle, F. 1957, *Rev. Mod. Phys*, 29, 547
- Busso, M., Gallino, R., & Wasserburg G. J. 1999, *ARA&A*, 37, 239
- Busso, M., Gallino, R., Lambert, D. L., Travaglio, C., & Smith V. V. 2001, *ApJ*, 557, 802
- Cowan, J. J., Thielemann, F.-K., & Truran, J. W. 1991, *Phys. Rep.*, 208, 267

- Cowan, J. J., et al. 1999, *ApJ*, 521, 194
- Cowan, J. J., et al. 2005, *ApJ*, 627, 238
- Cowan, J.J., & Sneden, C. 2006, *Nature*, 440, 1151C
- D’Ercole, A., & Brighenti, F. 1999, *MNRAS*, 309,941
- de Boer, T. J. L., et al. 2012, *A&A*, 544, 73
- Dutton, A. A., Mendel, J. T., & Simard, L. 2012, *MNRAS Letters*, 422, L33
- Feltzing, S., Fohlman, M., & Bensby, T. 2007, *A&A*, 467, 665
- Heger, A., & Woosley, S. E. 2010, *ApJ*, 724, 341
- Honda, S., Aoki, W., Kajino, T., Ando, H., Beers, T. C., Izumiura, H., Sadakane, K., Takada-Hidai, M. 2004, *ApJ*, 607, 474
- Irwin, M., & atzidimitriou, D. 1995, *MNRAS*, 277, 1354
- Ishimaru, Y., Wanajo, S., Aoki, W., Ryan, S. G. and Prantzos, N. 2005, *Nucl. Phys. A*, 758, 603
- Izutani, N., Umeda, H., Tominaga, N. 2009, *ApJ*, 692, 1517
- Johnson, J. 2002, *ApJS*, 139, 219
- Käppeler, F., Beer, H., & Wisshak, K. 1989, *Rep. Prog. Phys.*, 52, 945
- Kobayashi, C., Umeda, H., Nomoto, K., Tominaga, N., Ohkubo, T. 2006, *ApJ*, 653, 1145
- Lanfranchi, G. A., & Matteucci, F., 2003, *MNRAS*, 345, 71
- Lanfranchi, G. A., Matteucci, F., Cescutti, G. 2006, *MNRAS*, 365, 477
- Lanfranchi, G. A., & Matteucci, F. 2007, *A&A*, 468, 927
- Lanfranchi, G. A., Matteucci, F., Cescutti, G. 2008, *A&A*, 481, 635
- Letarte, B., et al. 2010, *A&A*, 523, 17
- Li, H. J., Shen, X. J., Liang, S., Cui, W. Y. & Zhang, B. 2013, *PASP*, 125, 143
- Mateo, M., Olszewski, E., Welch, D. L., Fischer, P., & Kunkel, W. 1991, *AJ*, 102, 914
- Matteucci, F., & Chiosi, C. 1983, *A&A*, 123, 121

- Mishenina, T.V., & Kovtyukh, V.V. 2001, *A&A*, 370, 951
- Mishenina, T.V., Kovtyukh, V.V., Soubiran, C., Travaglio, C., Busso, M. 2002, *A&A*, 396, 189
- Montes, F., et al. 2007, *ApJ*, 671, 1685
- Ono, M., Hashimoto, M., Fujimoto, S., Kotake, K., Yamada, S. 2012, *Progress of Theoretical Physics*, 128, 741
- Pignatari M., Gallino R., Hell, M., Wiescher, M., Käppeler, F., Herwig, F., Bisterzo, S. 2010, *ApJ*, 710, 1557
- Qian, Y.-Z., & Wasserburg, G. J., 2002, *ApJ*, 567, 515
- Qian, Y.-Z., & Wasserburg, G. J., 2007, *Phys. Rep.*, 442, 237
- Raiteri, C. M., Busso, M., Gallino, R., Picchio, G., & Pulone, L. 1991, *ApJ*, 371, 665
- Raiteri, C. M., Gallino, R., Busso, M. 1992, *ApJ*, 387, 263
- Raiteri, C. M., Gallino, R., Busso, M., Neuberger, D., & Käppeler, F. 1993, *ApJ*, 419, 207
- Reddy, B. E., Tomkin, J., Lambert, D. L., Allende Prieto, C. 2003, *MNRAS*, 340, 304
- Reddy, B. E., Lambert, D. L., Allend Prieto, C. 2006, *MNRAS*, 367, 1329
- Serminato, A., Gallino, R., Travaglio, C., Bisterzo, S., Straniero, O. 2009, *PASA*, 26, 153
- Shen, X. J., Zhang, B., Li, H. J., Shuai, L., Cui, W. Y. 2013, *Ap&SS*, 343, 541
- Shetrone, M., Wenn, K. A., Tolstoy, E., Primas, F., Hill, V., Kaufer, A. 2003, *AJ*, 125, 684
- Snedden, C., et al. 2003, *ApJ*, 591, 936
- Snedden, C., Cowan, J. J., & Gallino, R. 2008, *ARA&A*, 46, 241
- The, L.-S., El Eid, M. F., & Meyer, B. S. 2000, *ApJ*, 533, 998
- The, L.-S., El Eid, M. F., & Meyer, B. S. 2007, *ApJ*, 655, 1058
- Timmes F. X., Woosley S. E. & Weaver T. A. 1995, *ApJS*, 98, 617
- Tolstoy, E., Venn, K. A., Shetrone, M., Primas, F., Hill, V., Kaufer, A., Szeifert, T. 2003, *AJ*, 125, 707

- Travaglio, C., Galli, D., Gallino, R., Busso, M., Ferrini, F., & Straniero, O. 1999, *ApJ*, 521, 691
- Travaglio, C., Gallino, R., Arnone, E., Cowan, J., Jordan, F., & Sneden, C. 2004, *ApJ*, 601, 864
- Truran, J. W., Cowan, J. J., Pilachowski, C. A., Sneden, C. 2002, *PASP*, 114, 1293
- Tsujimoto, T. 2011, *ApJ*, 736, 113
- Walker, M. G., Mateo, M., Olszewski, E. W., Bernstein, R., Wang, X., Woodroffe, M. 2006, *AJ*, 131, 2114
- Wanajo S., & Ishimaru, Y. 2006, *Nucl. Phys. A*, 777, 676
- Westin, J., Sneden, C., Gustafsson, B., Cowan, J. J. 2000, *ApJ*, 530, 783
- Woosley, S. E., & Weaver, T. A. 1995, *ApJS*, 101, 181
- Woosley, S. E., Heger, A., & Weaver, T. A. 2002, *Reviews of Modern Physics*, 74, 1015

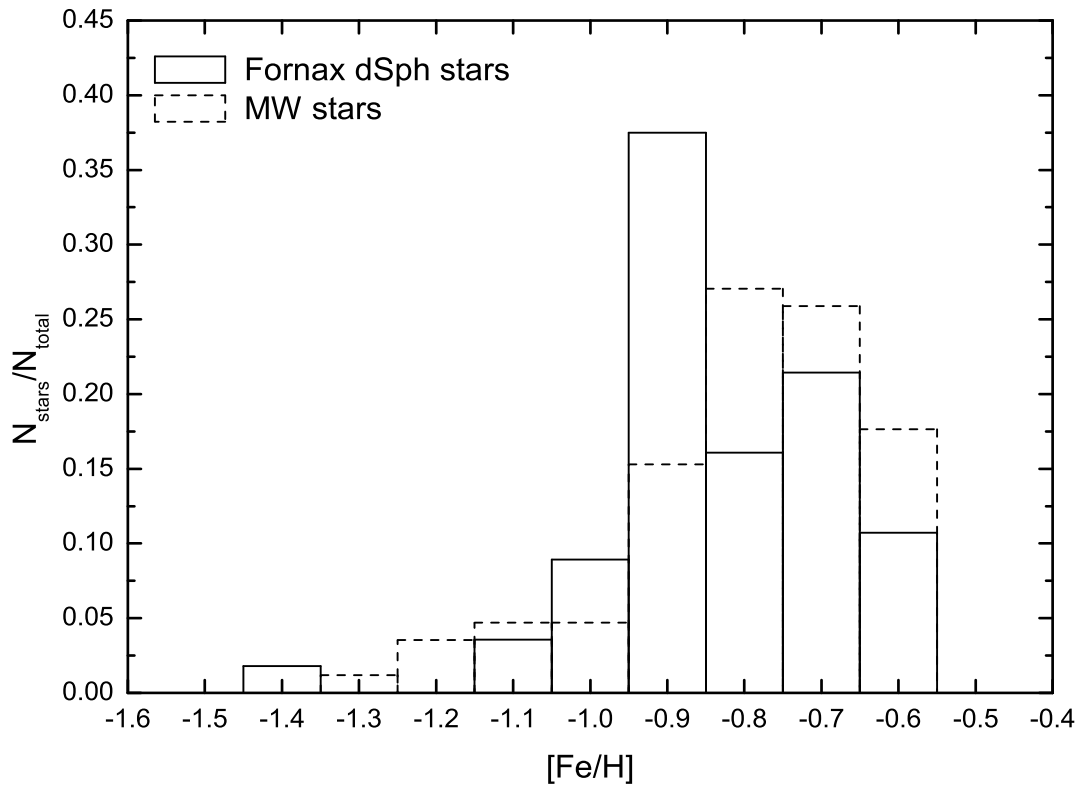


Fig. 1.— Metallicity distribution in the Fornax dSph stars (solid lines) compared to that of the MW stars (dash lines).

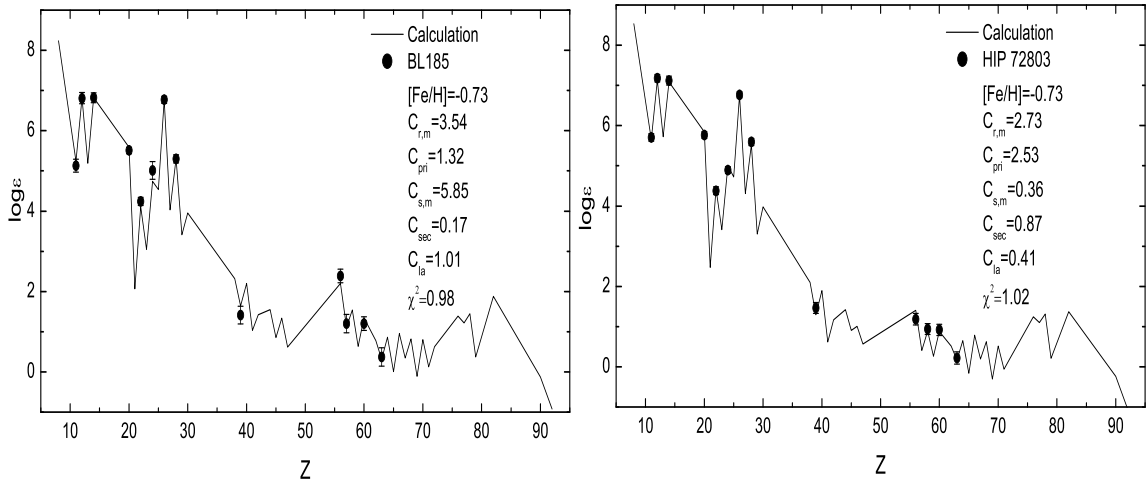


Fig. 2.— Two examples of calculated best-fitting results for the sample stars. The solid lines represent the calculated results. The observed elemental abundances are marked by filled circles. The left panel is one of the Fornax dSph stars. The right panel is a MW star.

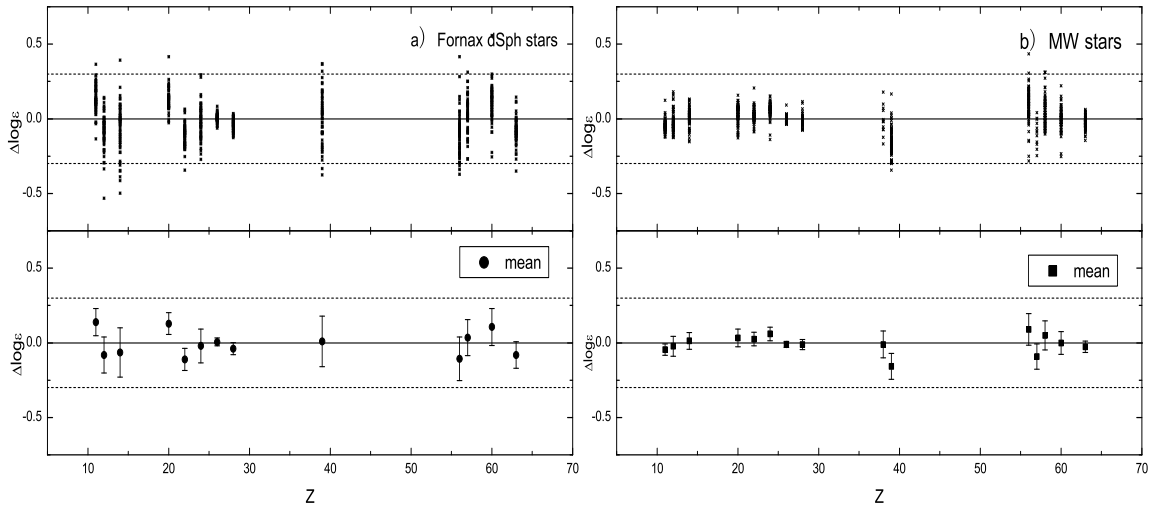


Fig. 3.— Top panels: individual relative offsets ($\Delta \log \varepsilon(X)$) for the Fornax dSph stars (stars) and MW stars (crosses). Typical observational uncertainties in $\log \varepsilon$ are $\sim 0.2 - 0.3$ dex (dash lines). Bottom panels: The root-mean-square offsets in $\log \varepsilon$ for the Fornax dSph stars (filled circles) and MW stars (filled squares).

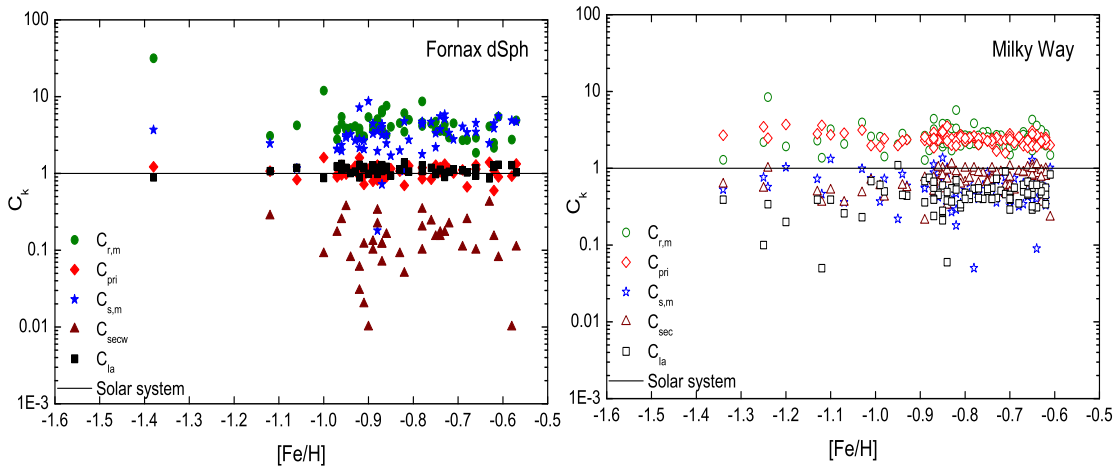


Fig. 4.— The component coefficients as a function of metallicity. In the left panel, filled circles, filled diamonds, filled stars, filled triangles and filled squares are the component coefficients of the main r-process, primary process, the main s-process, secondary process, and SNe Ia component respectively, for Fornax dSph stars. In the right panel, open circles, open diamonds, open stars, open triangles and open squares represent the component coefficients of the main r-process, primary process, the main s-process, secondary process, and SNe Ia component, respectively, for MW stars. The solid line presents the component coefficients of the solar system.

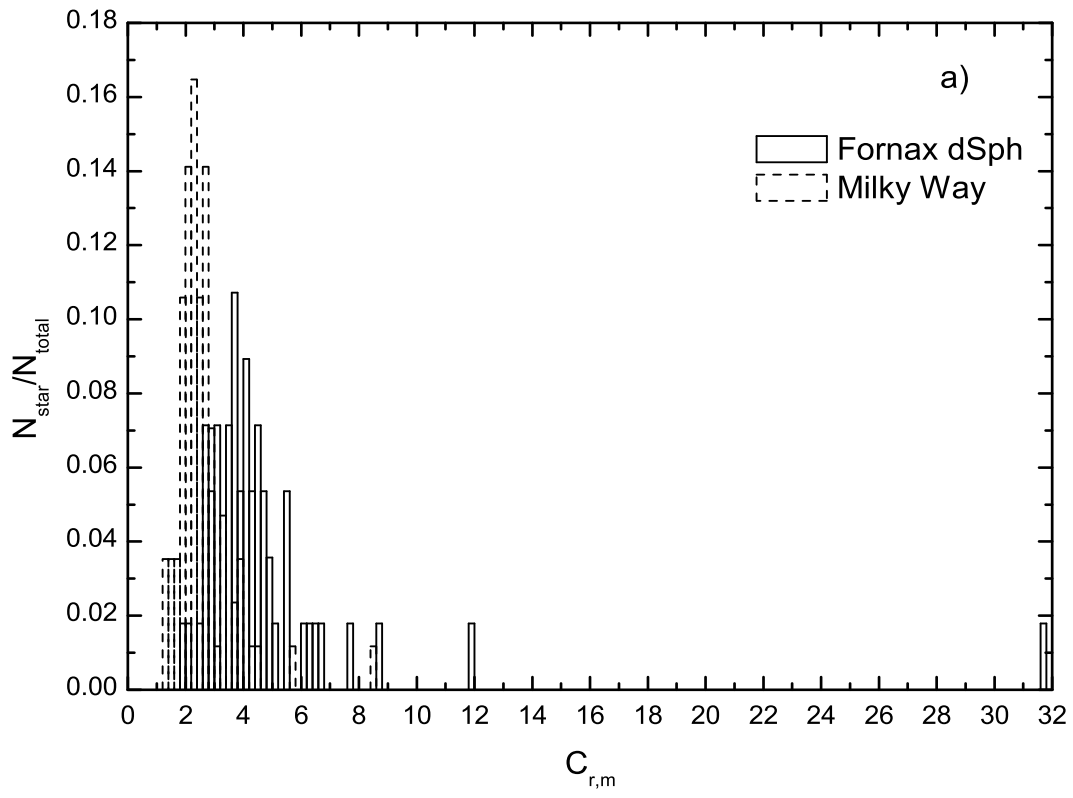


Fig. 5.— Five component coefficient distributions. The solid lines represent the Fornax dSph stars. The dash lines represent the MW stars.

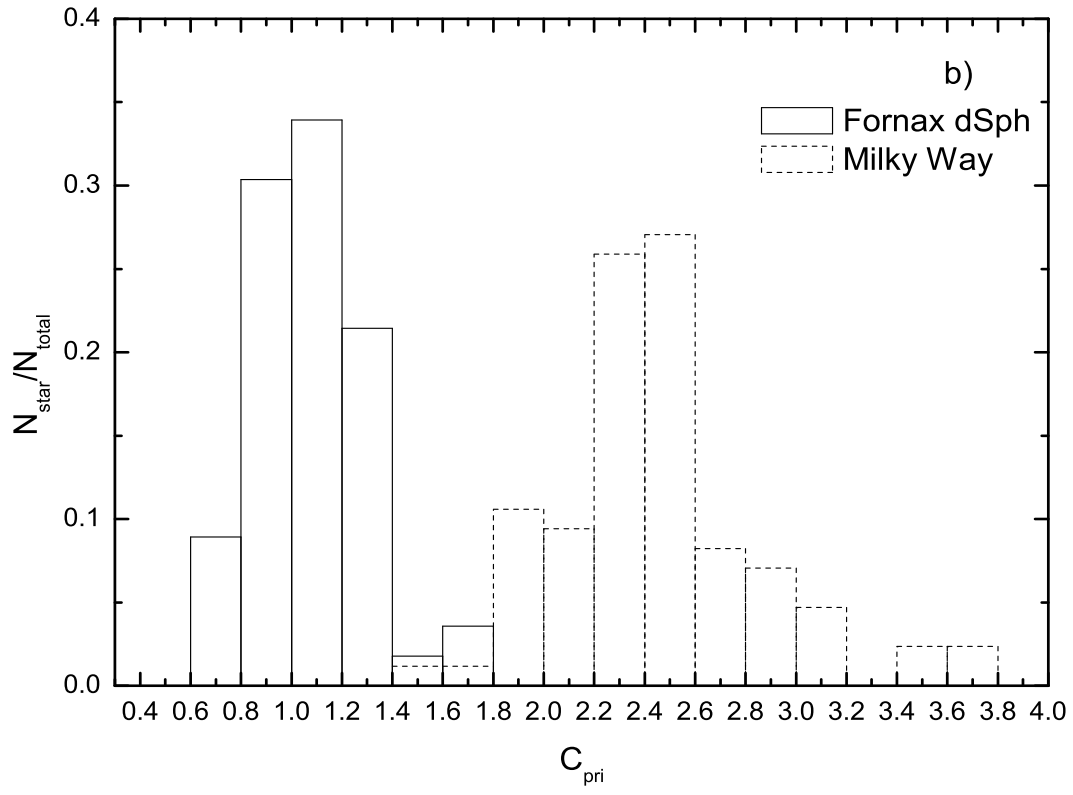


Fig. 5 (continued).

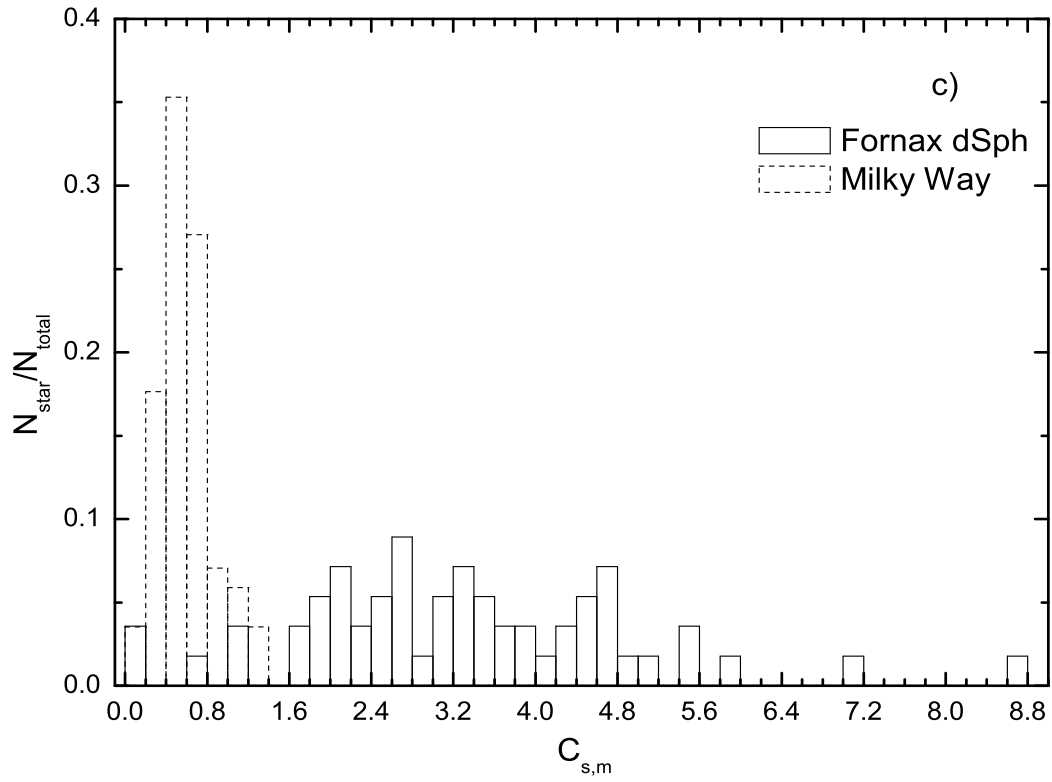


Fig. 5 (continued).

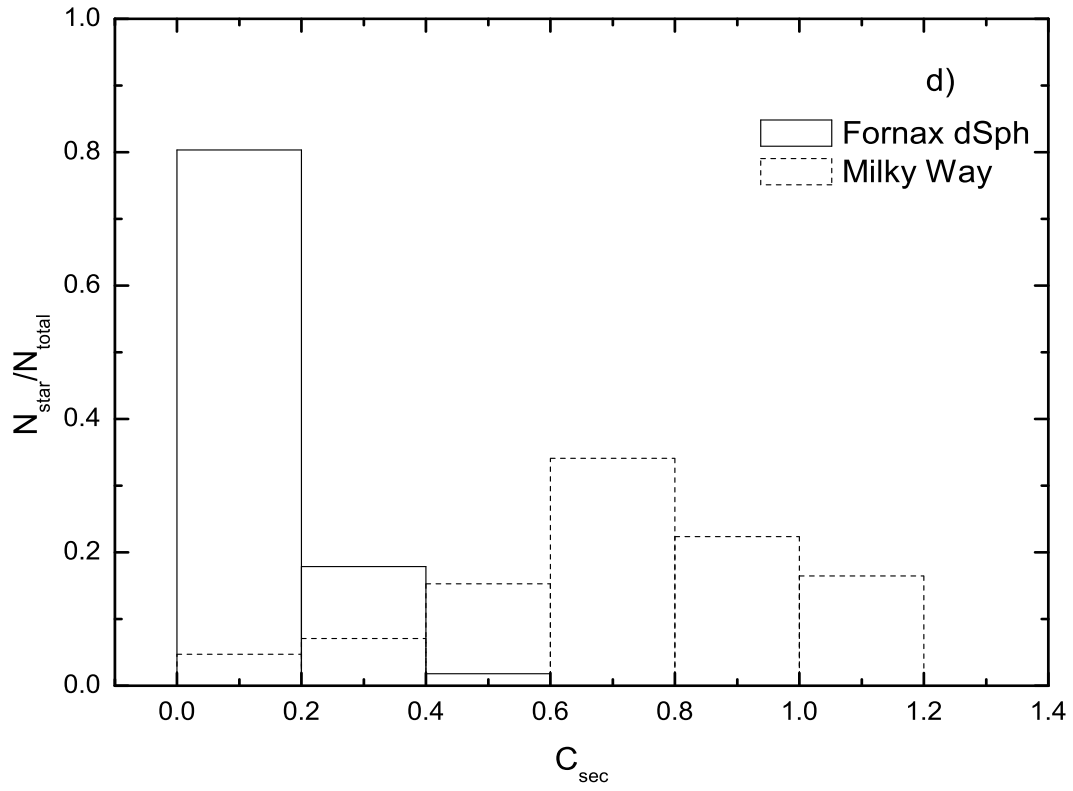


Fig. 5 (continued).

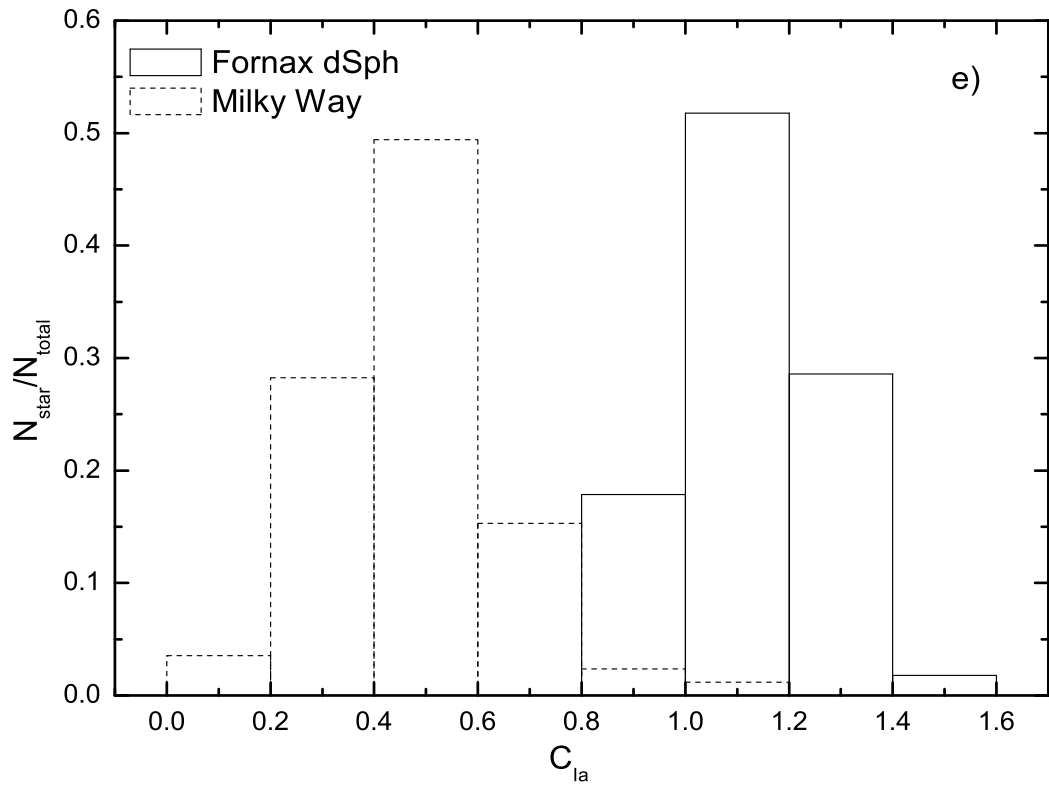


Fig. 5 (continued).

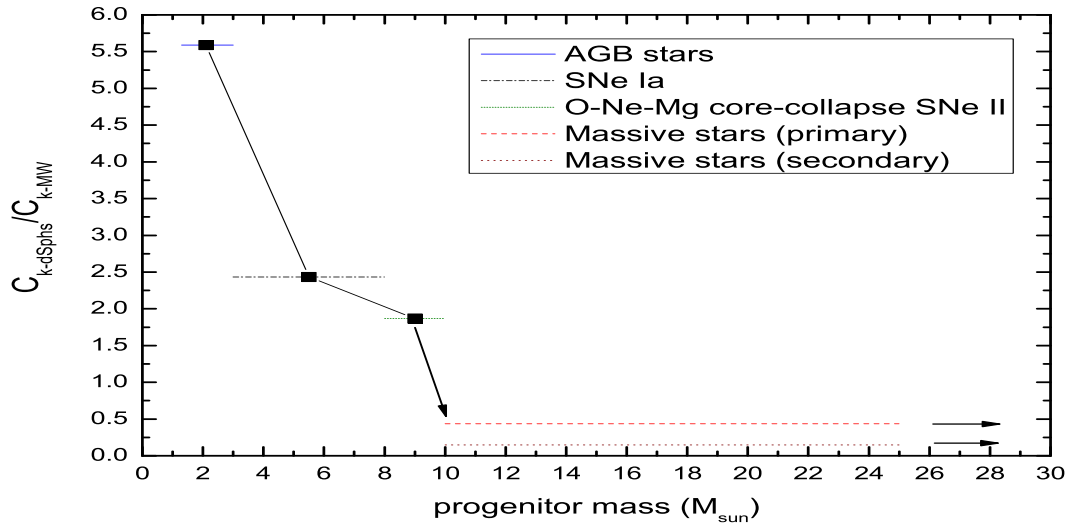


Fig. 6.— Ratios of the average component coefficient between the dSph stars and the MW stars as a function of progenitor mass. The solid line, short dotted line, dash line and dotted line represent the progenitor mass rang responsible to main s-process, main r-process, primary process and secondary process, respectively. The dash dotted line is the progenitor mass rang of SNe Ia. The filled square represents the average progenitor mass where the corresponding process mainly occurs.

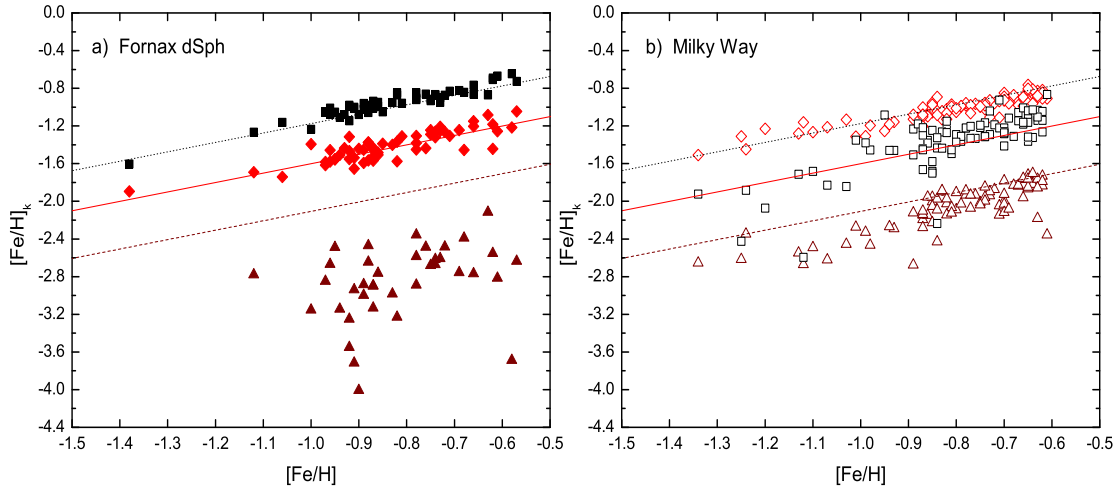


Fig. 7.— Component ratios of the individual process with various metallicities for element Fe. The component ratios of the dSph stars are shown in the left panel, in which the filled squares, filled diamonds and filled triangles are the component ratios of SNe Ia, primary-like yields and secondary-like yields, respectively. The ratios of the MW stars are shown in the right panel, in which the open squares, open diamonds and open triangles are the component ratios of SNe Ia, primary-like yields and secondary-like yields, respectively. In panels(a)and(b), solid lines, dash lines and dotted lines represent the solar component ratios of primary-like yields, secondary-like yields and SNe Ia, respectively.

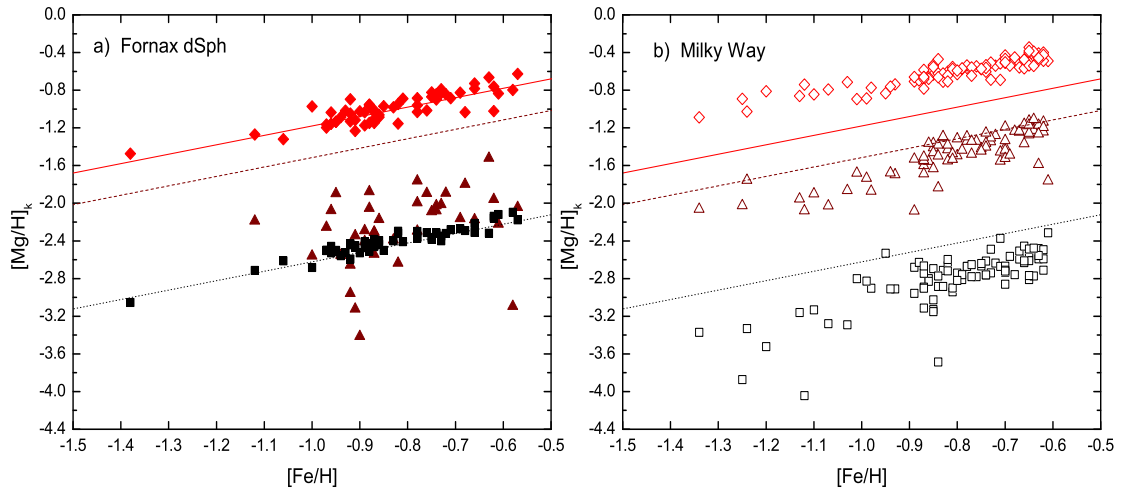


Fig. 8.— Component ratios of the individual process with various metallicities for element Mg. The component ratios of the dSph stars and the MW stars are shown in the left panel and right panel, respectively. The symbols are the same as Fig. 7.

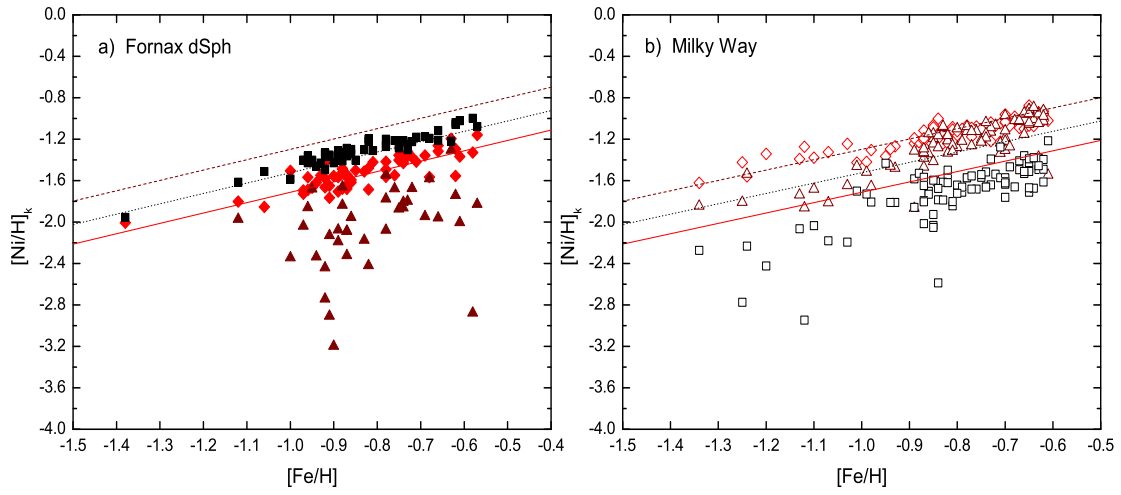


Fig. 9.— Component ratios of the individual process with various metallicities for element Ni. The component ratios of the dSph stars and the MW stars are shown in the left panel and right panel, respectively. The symbols are the same as Fig. 7.

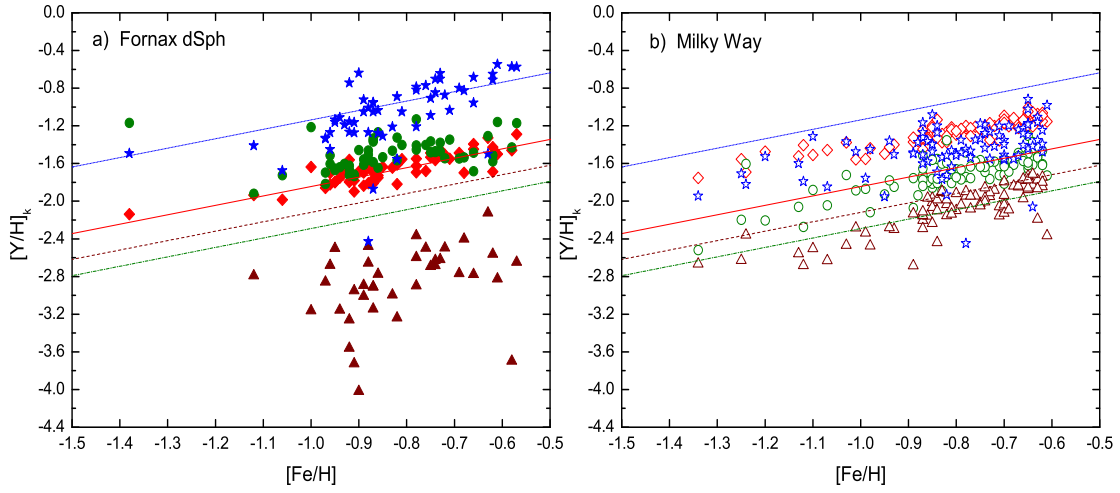


Fig. 10.— Component ratios of the individual process with various metallicities for element Y. The component ratios of the dSph stars are shown in the left panel, in which the filled circles, filled diamonds, filled stars and filled triangles are the component ratios of main r-process, weak r-process, main s-process and weak s-process, respectively. The ratios of the MW stars are shown in the right panel, in which the open circles, open diamonds, open stars and open triangles are responsible to main r-process, weak r-process, main s-process and weak s-process, respectively. In panels(a)and(b), dash dotted lines, solid lines, short dotted lines and dash lines represent the solar component ratios of main r-, weak r-, main s- and weak s-process, respectively.

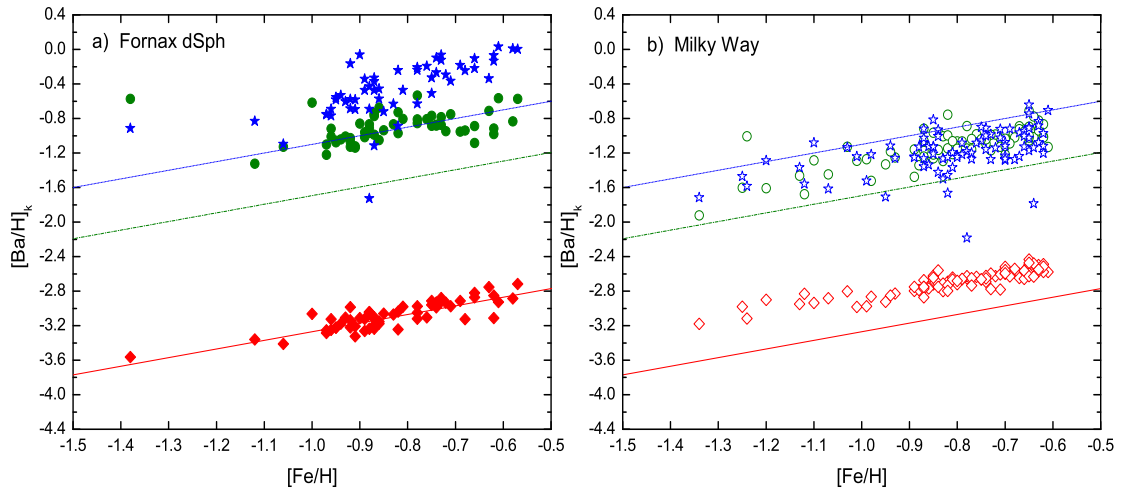


Fig. 11.— Component ratios of the individual process with various metallicities for element Ba. The component ratios of the dSph stars and the MW stars are shown in the left panel and right panel, respectively. The symbols are similar with Fig. 10.

Table 1: The five component coefficients, χ^2 and $K - K_{free}$ for the Fornax dSph stars.

Star	[Fe/H]	$C_{r,m}$	C_{pri}	$C_{s,m}$	C_{sec}	C_{Ia}	χ^2	$K - K_{free}$
BL038	-0.88	5.10	1.28	3.55	0.22	1.13	1.88	8
BL079	-0.57	4.90	1.33	4.73	0.11	1.04	0.49	8
BL081	-0.62	2.15	0.60	3.87	0.15	1.22	2.65	8
BL091	-0.96	4.43	0.96	1.96	0.25	1.33	0.62	8
BL092	-0.95	3.71	0.99	3.13	0.00	1.18	1.97	8
BL096	-0.75	4.74	1.15	2.20	0.00	1.02	0.75	8
BL097	-0.92	3.86	1.13	2.16	0.03	1.30	1.22	8
BL104	-0.96	5.45	1.27	2.34	0.00	1.14	2.40	8
BL113	-0.75	3.62	1.28	3.34	0.15	0.98	0.62	8
BL123	-0.97	3.66	0.90	2.09	0.17	1.23	1.95	8
BL125	-0.73	4.37	1.20	5.11	0.00	0.90	1.15	8
BL135	-0.95	3.86	0.99	2.94	0.37	1.16	2.03	8
BL140	-0.87	6.41	0.88	3.16	0.07	1.28	1.97	8
BL141	-0.82	3.50	0.70	1.08	0.00	1.33	0.86	8
BL146	-0.92	3.06	0.93	2.78	0.00	1.26	3.21	8
BL147	-1.38	31.69	1.22	3.69	0.00	0.89	1.96	8
BL148	-0.63	4.09	1.40	2.47	0.42	0.86	1.54	8
BL149	-0.91	2.92	0.94	2.67	0.02	1.17	1.35	8
BL155	-0.74	3.57	1.20	5.53	0.17	1.12	0.90	8
BL158	-0.87	6.69	0.80	4.37	0.12	1.26	2.06	8
BL160	-0.93	4.13	1.24	2.67	0.00	1.06	1.29	8
BL163	-0.78	4.60	1.00	4.37	0.20	1.12	1.09	8
BL166	-0.89	3.69	1.09	4.44	0.13	1.10	0.84	8
BL168	-0.88	4.61	1.27	1.95	0.33	0.99	1.24	8
BL173	-0.86	3.19	0.95	2.45	0.16	1.11	0.96	8
BL180	-0.9	5.42	1.14	8.71	0.01	0.99	0.40	8
BL185	-0.73	3.54	1.32	5.85	0.17	1.01	0.98	8
BL196	-1.06	4.22	0.83	1.16	0.00	1.18	1.54	8
BL197	-0.89	4.20	0.79	3.31	0.10	1.27	2.12	8
BL203	-0.83	4.54	1.07	1.99	0.09	1.13	0.32	8
BL204	-1	11.94	1.61	0.00	0.09	0.87	0.42	8
BL205	-0.69	2.71	1.11	4.06	0.11	1.10	0.34	8
BL208	-0.66	1.86	1.29	3.48	0.00	0.94	1.21	8
BL210	-0.76	4.44	0.84	4.66	0.24	1.18	2.14	8
BL211	-0.66	2.92	1.14	4.52	0.10	1.17	2.25	8
BL213	-0.94	3.90	1.08	3.23	0.08	1.01	1.33	8
BL216	-0.78	4.16	1.19	4.70	0.34	1.08	1.18	8
BL218	-0.62	2.50	1.09	4.47	0.00	1.27	1.24	8
BL221	-0.86	7.61	0.90	3.19	0.00	1.22	0.79	8

Star	[Fe/H]	$C_{r,m}$	C_{pri}	$C_{s,m}$	C_{sec}	C_{Ia}	χ^2	$K - K_{free}$
BL227	-0.87	6.22	1.09	3.98	0.12	1.08	1.33	8
BL228	-0.88	4.04	0.82	0.18	0.00	1.19	3.75	8
BL229	-0.71	4.51	1.01	2.78	0.00	1.13	0.82	8
BL233	-0.68	2.73	0.67	3.43	0.25	1.03	2.08	8
BL242	-1.12	3.09	1.07	2.45	0.28	1.07	2.41	8
BL247	-0.82	6.10	1.13	4.77	0.05	1.40	3.54	8
BL253	-0.74	3.64	1.05	3.74	0.15	1.10	1.02	8
BL257	-0.58	2.76	0.92	4.87	0.01	1.28	1.18	8
BL258	-0.61	5.50	0.90	5.53	0.08	1.30	0.44	8
BL260	-0.87	3.77	1.05	0.72	0.00	1.11	1.31	8
BL261	-0.85	4.04	1.15	1.70	0.00	0.94	1.48	8
BL267	-0.72	2.93	1.14	3.36	0.22	1.05	0.56	8
BL269	-0.81	4.99	1.26	2.75	0.00	1.06	1.44	8
BL300	-0.92	3.50	1.60	7.19	0.06	0.89	1.78	8
BL304	-0.97	2.77	0.97	2.06	0.00	1.24	1.53	8
BL311	-0.78	8.69	0.85	1.78	0.10	1.27	0.80	8
BL323	-0.91	3.04	0.72	2.08	0.12	1.21	2.23	8

Table 2: The five component coefficients, χ^2 and $K - K_{free}$ for the MW stars.

Star	[Fe/H]	$C_{r,m}$	C_{pri}	$C_{s,m}$	C_{sec}	C_{Ia}	χ^2	$K - K_{free}$
HD 245	-0.78	3.86	2.50	0.05	0.90	0.54	0.97	6
HD 3546	-0.63	2.48	2.52	0.45	0.36	0.59	0.20	6
HD 6833	-0.89	1.28	2.30	0.56	0.21	0.68	0.78	6
HD 64606	-0.82	2.33	2.50	0.29	0.80	0.60	0.61	6
HD 105755	-0.65	1.70	3.06	1.28	0.00	0.49	0.76	6
HD 108076	-0.85	1.92	2.49	1.37	0.90	0.60	1.50	6
HD 127243	-0.65	1.94	2.50	0.71	1.00	0.46	0.34	6
HD 166161	-1.20	1.93	3.71	1.03	0.00	0.20	1.45	6
HD 204155	-0.78	2.12	2.65	0.50	1.00	0.54	2.41	6
HD 208906	-0.71	2.36	1.58	0.77	0.47	0.91	0.82	6
HD 224930	-0.85	2.12	3.08	0.67	1.00	0.28	2.17	6
HD 165908	-0.61	1.49	2.00	1.01	0.23	0.83	1.22	5
HD 221377	-0.88	1.71	2.31	0.71	0.00	0.75	1.50	5
HIP 3185	-0.65	4.32	2.68	0.38	1.09	0.29	0.53	8
HIP 5122	-0.62	2.80	2.05	0.40	0.99	0.56	0.49	8
HIP 5336	-0.86	2.30	2.39	0.42	1.03	0.48	0.55	8
HIP 6159	-0.67	2.97	2.20	0.64	0.87	0.50	0.78	8
HIP 7961	-0.64	2.08	2.69	0.40	0.85	0.31	0.42	8
HIP 12579	-0.80	2.69	2.24	0.47	0.66	0.48	0.75	8
HIP 13366	-0.70	2.41	2.55	0.33	0.65	0.39	0.60	8
HIP 15405	-0.73	1.80	1.67	0.70	0.79	0.73	0.24	8
HIP 17147	-0.87	2.74	2.93	0.78	0.61	0.24	1.08	8
HIP 17666	-1.03	3.96	3.14	0.99	0.48	0.23	1.00	8
HIP 22060	-0.63	2.43	2.14	0.79	0.94	0.46	1.47	8
HIP 29269	-0.68	2.27	2.56	0.32	0.91	0.35	0.33	8
HIP 39893	-0.84	3.78	2.50	0.33	0.94	0.38	0.74	8
HIP 40613	-0.62	2.02	2.52	0.33	0.78	0.34	0.80	8
HIP 44075	-0.86	2.27	2.30	0.69	0.66	0.45	0.66	8
HIP 44347	-0.85	3.80	3.14	0.66	0.54	0.22	0.76	8
HIP 52673	-0.66	2.66	2.31	0.65	1.00	0.45	0.75	8
HIP 59233	-0.83	1.70	2.44	0.27	1.10	0.37	0.76	8
HIP 60268	-0.72	2.69	2.30	0.48	0.90	0.51	0.36	8
HIP 62240	-0.83	3.30	2.00	0.46	1.13	0.55	1.84	8
HIP 64426	-0.71	1.89	2.37	0.61	0.59	0.46	0.69	8
HIP 70520	-0.62	1.97	2.37	0.56	0.87	0.45	0.40	8
HIP 72803	-0.73	2.73	2.53	0.36	0.87	0.41	1.02	8
HIP 74033	-0.85	2.39	2.99	0.55	0.80	0.21	0.92	8
HIP 74067	-0.75	2.99	2.26	0.62	0.70	0.51	0.82	8

Star	[Fe/H]	$C_{r,m}$	C_{pri}	$C_{s,m}$	C_{sec}	C_{Ia}	χ^2	$K - K_{free}$
HIP 85757	-0.70	1.50	2.82	0.53	0.76	0.29	0.65	8
HIP 86013	-0.70	2.74	2.35	0.48	0.60	0.45	0.92	8
HIP 88039	-0.81	1.96	2.74	0.52	0.71	0.31	1.08	8
HIP 88166	-0.76	2.95	2.48	0.60	0.86	0.40	1.19	8
HIP 98532	-1.13	2.29	2.82	0.73	0.49	0.39	0.88	8
HIP 112811	-0.70	1.88	2.58	0.37	0.49	0.41	1.06	8
HIP 113514	-0.63	3.17	2.24	0.70	0.76	0.50	0.70	8
HIP 117029	-0.77	2.02	2.46	0.47	0.88	0.41	0.64	8
HIP 4039	-1.24	8.45	2.47	0.57	1.00	0.34	0.81	6
HIP 4544	-0.87	4.41	2.45	0.51	0.68	0.40	1.79	7
HIP 10652	-0.67	2.75	1.96	0.34	0.89	0.61	0.39	7
HIP 15126	-0.82	3.30	2.27	0.47	0.61	0.53	0.44	6
HIP 26452	-0.89	2.66	2.57	0.55	0.75	0.36	0.97	7
HIP 27128	-0.81	2.76	2.60	0.35	0.62	0.34	1.24	7
HIP 36849	-0.77	2.68	2.02	0.40	0.64	0.55	0.78	7
HIP 38769	-0.79	2.05	2.49	0.47	0.74	0.40	0.52	7
HIP 58843	-0.79	2.62	2.52	0.64	0.74	0.45	0.86	8
HIP 59750	-0.74	2.19	2.43	0.69	0.78	0.40	1.24	6
HIP 70681	-1.10	3.23	2.72	1.32	0.52	0.39	1.21	7
HIP 85373	-0.82	5.72	1.96	0.18	0.90	0.70	2.88	7
HIP 104659	-1.07	2.07	2.87	0.36	0.36	0.26	1.12	6
HIP 110291	-0.93	2.36	2.36	0.59	0.56	0.44	1.24	7
HIP 14086	-0.65	2.81	2.80	0.53	0.78	0.32	0.84	8
HIP 10449	-0.87	3.22	2.34	0.88	0.50	0.56	0.38	7
HIP 28671	-1.01	2.60	1.98	0.74	0.70	0.68	0.92	6
HIP 55592	-0.94	2.83	2.28	0.84	0.60	0.45	0.83	7
HIP 62882	-0.98	1.42	2.43	0.73	0.42	0.50	0.55	8
HIP 78640	-1.34	1.29	2.70	0.53	0.62	0.39	0.39	5
HIP 80837	-0.80	2.21	2.45	0.45	1.00	0.40	0.68	8
HIP 86321	-0.87	2.44	1.85	1.12	0.69	0.67	0.37	6
HIP 94449	-1.12	1.37	3.63	0.46	0.36	0.05	0.58	7
HIP 100568	-0.99	2.58	1.92	0.37	0.59	0.61	0.39	8
HIP 111549	-0.95	2.05	1.98	0.22	0.00	1.10	1.31	6
HIP 5163	-0.74	2.51	2.08	0.85	1.00	0.56	0.59	7
HIP 8720	-0.74	2.47	2.28	0.48	0.71	0.40	1.13	8
HIP 10711	-0.69	1.97	2.14	0.74	0.52	0.56	0.70	7
HIP 21306	-0.65	2.10	2.11	1.01	0.81	0.56	0.71	8
HIP 30990	-0.87	2.10	2.45	0.41	0.75	0.39	0.67	7
HIP 42734	-0.70	2.29	2.38	0.34	1.06	0.40	0.22	8
HIP 80162	-0.66	2.52	1.87	0.57	1.03	0.67	1.21	8

Star	[Fe/H]	$C_{r,m}$	C_{pri}	$C_{s,m}$	C_{sec}	C_{Ia}	χ^2	$K - K_{free}$
HIP 20298	-0.84	2.10	3.54	1.02	0.33	0.06	1.21	8
HIP 23922	-0.66	2.38	2.32	0.43	0.64	0.47	0.99	8
HIP 26617	-0.75	2.54	2.28	0.89	0.66	0.54	0.58	8
HIP 43595	-0.84	2.35	2.28	0.86	0.72	0.49	0.69	8
HIP 48209	-0.65	2.24	1.96	0.69	0.99	0.61	0.54	8
HIP 51477	-1.25	2.20	3.46	0.76	0.55	0.10	1.77	8
HIP 60331	-0.64	3.61	1.90	0.09	1.11	0.61	1.63	7